Dynamic Resource Allocation for LTE-Based Vehicle-to-Infrastructure Networks

Jianfeng Shi, *Student Member, IEEE*, Zhaohui Yang, *Student Member, IEEE*, Hao Xu, *Student Member, IEEE*, Ming Chen, *Member, IEEE*, and Benoit Champagne, *Senior Member, IEEE*

***Abstract*—This paper studies the dynamic resource allocation (DRA) problem for LTE-based vehicle-to-infrastructure networks, where the goal is to minimize the total power consumption (TPC) in the downlink, subject to both power constraints and rate requirements. Under time-varying channel conditions, the TPC minimization takes the form of a discrete-time sequence of NP-hard combinational optimization problems. To solve these sequential problems, we propose a novel two-stage algorithm, named as DRA and precoding algorithm (DRA-Pre). In the first stage, the resource allocation problem (i.e., pairing of vehicle users to roadside units, and subcarrier allocation) is solved by applying the multi-value discrete particle swarm optimization method. This approach takes advantage of the channel correlation by exploiting the relationship between resource allocation solutions in adjacent time slots, which can improve the TPC performance. In the second stage, the precoding design problem is solved by a low-complexity algorithm, where the original problem is split into two subproblems, i.e., a rate max–min subproblem and a TPC minimization subproblem. Simulation results show that the proposed algorithm converges rapidly and significantly outperforms benchmark approaches in terms of TPC.**

***Index Terms*—Dynamic resource allocation, LTE-based V2I networks, mutlivalue discrete particle swarm optimization (MDPSO), multi-antenna transceiver.**

I. Introduction

VEHICULAR networking is one of the key technologies underlying the implementation of intelligent transportation systems (ITS) [1]. While WAVE (IEEE 802.11p) is a popular wireless access technology that can provide the required radio interface, it suffers from a number of drawbacks, including poor scalability, low capacity and intermittent connectivity [2]. Hence, LTE-based wireless vehicular networking has attracted great attention from both academia and industry [2], [3]. In general, LTE-based vehicular networks encompass four different types of communication scenarios: vehicle-to-infrastructure (V2I), vehicle-to-network (V2N), vehicle-to-vehicle (V2V), and vehicle-to-pedestrian (V2P). On the one hand, due to the wide deployment of existing LTE networks, V2I and V2N communications can provide high data rate, comprehensive quality of service (QoS) support, ubiquitous coverage, and high penetration rate. On the other hand, V2V and V2P communications over shorter distances can be realized by means of device-to-device (D2D) techniques [3].

In LTE-based V2I networks, vehicle user equipments (VUEs) exchange information with roadside units (RSUs), while all RSUs are connected to the eNodeB (eNB) via high speed and low-latency links. Compared with IEEE 802.11p, LTE-based V2I networks inherit the advantages of LTE, including support of V2I, high mobility, robustness to congestion, higher multiplexing capacity, wider coverage and flexible resource management [2], [4].

Despite these remarkable advantages, several technical challenges remain for LTE-based vehicular networks [5]–[7]. Specifically:

1) satisfying stringent reliability and low latency to guarantee a better user experience;
2) designing efficient resource allocation schemes to meet diverse requirements in terms of bandwidth, power consumption, energy efficiency, etc.;
3) implementing data-centric trust and verification mechanisms to protect the network from in-transit traffic tampering and other security threats or attacks;
4) ensuring a trade-off among authentication, privacy, and liability when the network has to disclose user information to governing authorities.

The need for efficient solutions to these challenges is pressing, especially in light of the tremendous and swift increase in V2I data traffic predicted over the coming years [8]. Accordingly, in this paper, we focus on the problem of dynamic resource allocation in high mobility[1] environments for LTE-based V2I networks.

Manuscript received May 3, 2018; revised January 20, 2019; accepted March 4, 2019. Date of publication March 8, 2019; date of current version May 28, 2019. This work was supported in part by the National Science and Technology Major Project under Grant 2016ZX03001016-003, in part by the National Natural Science Foundation of China under Grants 61871128, 61372106, and 61221002, in part by the Nature Science Foundation of Jiangsu Province under Grant BK20170557, in part by the Nature Science Foundation for Higher Education Institutions of Jiangsu Province of China under Grant 17KJB510009, in part by the Open Research Fund of National Mobile Communications Research Laboratory, Southeast University under Grant 2018D13, and in part by the China Scholarship Council for a 1-year fellowship to McGill University and the NSERC of Canada. The review of this paper was coordinated by Dr. Z. Fadlullah. *(Corresponding author: Jianfeng Shi.)*

J. Shi, Z. Yang, H. Xu, and M. Chen are with National Mobile Communications Research Laboratory, Southeast University, Nanjing 210096, China (e-mail: shijianfeng@seu.edu.cn; yangzhaohui@seu.edu.cn; xuhao2013@seu.edu.cn; chenming@seu.edu.cn).

B. Champagne is with the Department of Electrical and Computer Engineering, McGill University, Montreal, QC H3A 0G4, Canada (e-mail: benoit.champagne@mcgill.ca).

Digital Object Identifier 10.1109/TVT.2019.2903822

[1]The high mobility of the VUEs poses major challenges from both perspectives of system design and implementation. For instance, the high speed poses stringent requirements on resource allocation and other network functions such as hand-off. Accordingly, research studies with special consideration of high mobility have received considerable attention from both industry and academia in recent years [9], [10].

A. Related Work

In [11], a joint spectrum access and power allocation problem was formulated, aiming to minimize the overall energy consumption while maintaining a given QoS in V2I uplink communications. A heuristic algorithm based on greedy strategy and the bisection method was then applied to tackle the ensuing mixed-integer non-linear problem (MINLP). Considering a similar system model, the authors in [12] addressed the channel allocation problem with the objective of maximizing system-wide throughput while maintaining QoS and latency requirements. To solve the resulting mixed-integer linear programming (MILP) problem, an interference-aware high-throughput channel allocation mechanism was proposed. With the same objective, a resource allocation problem was investigated in [13] while taking into account the interference between directional transmission beams. Based on the modified iterative water-filling, an iterative resource allocation method was proposed, while a heuristic scheme was devised to reduced the complexity.

The resource allocation problem was studied in [14]–[16] by considering two kinds of connections, i.e. V2V and V2I, concurrently. Specifically, in [14], a subchannel allocation method was proposed to increase the amount of spatial reuse of cellular radio resources. In addition, a power control scheme was devised to guarantee the transmission rate for every V2V link while minimizing the desired transmission power at each VUE. A resource allocation problem aiming to maximize the sum capacity of the V2I links was investigated in [15]. The authors developed a low-complexity algorithm to tackle the MINLP and obtained the optimal spectrum sharing strategy among V2I and V2V links, while properly adjusting their transmitting powers. Based on [15], the authors in [16] further formulated a optimization problem to maximize the ergodic capacity only based on partial channel state information and proposed robust algorithms.

While addressing different resource allocation problems for cellular networks (as opposed to the V2I network model under consideration here), an interesting body of recent works has focused on the application of discrete particle swarm optimization (DPSO) [17]–[20]. Specifically, in [17], [18], the allocation of subcarrier and transmit power among mobile stations (MS) in a cooperative cellular network was formulated as the maximization of an average utility function. Multi-value DPSO (MDPSO) was then proposed as an evolutionary algorithm to solve the resulting NP-hard combinatorial problem, making it possible to exploit correlation of radio parameters between adjacent frames. In [19], [20], the authors investigated the problem of load balancing, where the aim is to maximize the QoS of a multi-cell cloud radio access network (CRAN) via the mapping of remote radio heads (RRH) to baseband units (BBU). DPSO was applied to solve the RRH allocation and provided better performance than the genetic and exhaustive search algorithms.

B. Motivation and Contributions

The above mentioned works [11]–[16] only consider the case of single antenna. Yet, with the growth evolution of antenna technology, it is now favorable and in fact highly desirable to equip the VUE and RSU with multiple antennas. Although some problems were studied in the case of multi-antenna (e.g., beam and power allocation [21] and cooperative multiple-input multiple-output (MIMO) scheme selection [22]), they are quite different from our work. In addition, majority of the existing literature on resource allocation in vehicular networks consider this problem from a static optimization respective. In other words, when the radio channel conditions change over time, these resource allocation algorithms regard the changes as defining a brand new problem that must be solved from scratch, without considering the relationship between the different time slots. Intuitively, it should be possible to reduce algorithm complexity and improve the system performance significantly by exploiting knowledge available from the previous time slot. Besides, escalating energy consumption is a key issue for service providers and network operators as it may represent a significant portion of their operating costs. Accordingly, the notion of energy efficient, or green communications will play a central role in defining future generations of wireless network [23]. Hence, to address these challenges, this paper considers a multi-antenna case and study the *dynamic* resource allocation problem to minimize the total power consumption (TPC) in LTE-based V2I downlink networks, satisfying per-RSU power constraints and VUEs' rate requirements.

Specifically, we formulate the allocation problem as a NP-hard mixed integer-continuous variable optimization problem. In particular, we present an extensive analysis in two stages: dynamic resource allocation scheme based on MDPSO in the first stage; low-complexity precoding design based on the Lagrangian dual method in the second stage. While several dynamic resource allocation schemes have been developed in [18], [24], [25], with emphasis on LTE type networks, the problem in our work is different and more difficult in terms of the system model and design objectives. Due to major differences in network configuration, vehicular user dynamics and service type requirements in LTE-based V2I networks, these schemes cannot be readily applied to obtain the solution to our problem. For instance, the results from [18] cannot be applied directly because we consider the precoding matrix at the RSU instead of power allocation and focus on the V2I networks instead of relay-aided cooperative OFDMA systems. Another important limitations of existing approach in the V2I context is that they do not attempt to exploit channel state information across multiple time slots. Therefore, in this paper, we propose to tackle this NP-hard mixed integer-continuous variable optimization problem which we tackle via the application of MDPSO and optimization theory.

The major contributions of our work are summarized as follows:

1) Regarding the first stage, we characterize the relationship between the resource allocation in adjacent time slots for a time-varying radio environment. With given precoding matrices, we propose an MDPSO-based dynamic resource allocation algorithm that takes advantage of this relationship and analyze its computational complexity. Simulation results show that the proposed dynamic resource allocation algorithm converges rapidly.

TABLE I
LIST OF NOTATIONS

Symbols	Definitions
K	Number of RSUs
M	Number of VUEs
v_m	Moving speed of the mth VUE
N, W	Number of subcarriers and total bandwidth
N_t, N_r	Number of transmitting and receiving antennas
$\mathbf{V}_{km}^n$	Precoding matrix from the kth RSU to mth VUE on the nth subcarrier
$\mathbf{H}_{km}^n$	Channel matrix between the kth RSU and mth VUE on the nth subcarrier
$\mathbf{X}$ ($\mathbf{X}^l$)	RSU-VUE pairing and subcarrier allocation (at time slot l)
R_m (R_m^l)	Achievable data rate of the mth VUE (at time slot l)
$R^{\min}$	Minimum rate requirement
P_k (P_k^l)	Power consumption of the kth RSU (at time slot l)
P_{tot} (P_{tot}^l)	Power consumption of the whole network (at time slot l)
$P_k^{\max}$	Maximum power budget of the kth RSU
ΔX^l	Approximate distance between the optimal resource allocations at time slot l and $l-1$
I	Particle swarm size
$\boldsymbol{\chi}_i$	Position of the ith particle
$\mathbf{S}_i$	Velocity of the ith particle
pbest_i	Best position of the ith particle
gbest	Global best position

2) Regarding the second stage, we formulate and solve the precoding problem with given resource allocation. This problem is still non-convex because of rank constraints; moreover, due to the conflicting nature of the power constraints and rate requirements, the precoding problem may be infeasible. The rank constraint is addressed via a relaxation approach while to check feasibility, we divide the precoding problem into a max-min rate problem and a TPC minimization problem. If the obtained objective of the former satisfies the rate requirement (i.e., the precoding problem is feasible), we proceed to solve the latter. Based on the Lagrangian dual method, we propose two algorithms that allow us to solve subproblem in closed form. Simulation results indicate that the proposed algorithms possess good convergence performance.
3) By combining these two stages, we propose a dynamic resource allocation and precoding algorithm (DRA-Pre) to solve the TPC minimization problem in LTE-based V2I downlink networks. Simulation results indicate that our proposed DRA-Pre algorithm outperforms the benchmark methods over a wide range of dynamic conditions for the radio environment.

C. Organization

In Section II, we present the system model and formulate the TPC minimization problem. Section III develops an MDPSO-based dynamic resource allocation algorithm with given precoding matrix. Section IV proposes low-complexity algorithms to solve the precoding design problem with fixed resource allocation. Simulation results and discussions are presented in Section V. Finally, Section VI concludes this paper.

Notation: Uppercase and lowercase boldface denote matrices and vectors, respectively. For a matrix $\mathbf{A}$, $[\mathbf{A}]_{ij}$ means the (i,j)th element of $\mathbf{A}$, respectively. $(\cdot)^{\text{H}}$ and $\text{tr}(\cdot)$ denote Hermitian transpose and trace operator, respectively. $\|\mathbf{A}\|_{\text{F}}$, $\text{rank}(\mathbf{A})$ and $|\mathbf{A}|$ are the Frobenius-norm, rank value of $\mathbf{A}$, and its determinant. $\mathbf{I}_N$ is the $N \times N$ identity matrix. $\mathcal{CN}(\mathbf{a}, \mathbf{B})$ is a circularly symmetric complex Gaussian distribution with covariance matrix $\mathbf{B}$ and mean vector $\mathbf{a}$. For convenience, some important symbols are listed in Table I.

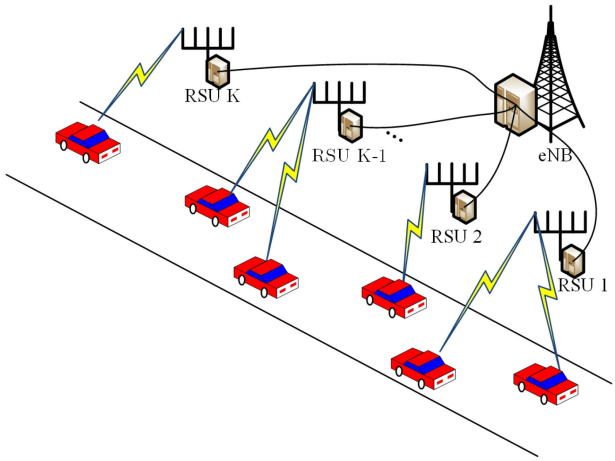

Fig. 1. Illustrative scenario of a (downlink) V2I network with one eNB, multiple RSUs, and VUEs. All RSUs are connected to the eNB with high-bandwidth dedicated links.

II. SYSTEM MODEL AND PROBLEM FORMULATION

In this section, we describe the adopted LTE-based V2I system model and formulate the TPC optimization problem. The key underlying assumptions assumptions are highlighted and explained.

A. MIMO System Description

We consider a downlink LTE-based V2I network with one eNodeB (eNB), K RSUs and M VUEs sharing a total number of N subcarriers spanning a bandwidth W, as illustrated in Fig. 1.

The RSUs, each equipped with N_t transmitting antennas, are uniformly distributed on the side of the road. They are connected to the eNB via high speed dedicated links (e.g., optical fiber), allowing centralized cloud-based processing. The VUEs, each equipped with N_r receiving antennas,[2] are assumed to move in the same direction for simplicity, but possibly at different speeds.

To simplify the analysis, we assume that near perfect channel state information is available at the transmitters, as obtained from efficient and accurate channel estimation methods such as those proposed in [28], [29]. To avoid inter-VUE interference and make the problem tractable, we assume that each VUE is served by a single RSU, and that each subcarrier can be allocated to at most one RSU-VUE pair. We further assume that every VUE can be served by the network, which require $N \geq M$. However, no specific relationship is imposed between K and M, which is suitable for practical scenarios.

The RSU-VUE pairing and subcarrier allocation scheme can be conveniently represented by the following matrix,

$$\mathbf{X} = \begin{bmatrix} a_1 & b_1 \\ \vdots & \vdots \\ a_n & b_n \\ \vdots & \vdots \\ a_N & b_N \end{bmatrix}, \; a_n \in \{0, 1, \ldots, K\}, \; b_n \in \{0, 1, \ldots, M\}, \tag{1}$$

where the pair (a_n, b_n) in the nth row signifies that the nth subcarrier is assigned to the a_nth RSU and the b_nth VUE. By convention, if one of a_n or b_n is equal to 0, the nth subcarrier is not assigned. We define π_{km}^n as the resource allocation indicator variable deduced from $\mathbf{X}$, i.e.,

$$\pi_{km}^n = \begin{cases} 1, & \text{if } a_n = k \text{ and } b_n = m, \\ 0, & \text{otherwise.} \end{cases} \tag{2}$$

Let $\mathbf{V}_{km}^n \in \mathbb{C}^{N_t \times N_s}$ represent the precoding matrix used at the kth RSU to send data symbol to the mth VUE on the nth subcarrier. According to [30], the number of data streams for each user is given by $N_s = \min\{N_t, N_r\}$. The channel matrix between the kth RSU and the mth VUE on the nth subcarrier is denoted by $\mathbf{H}_{km}^n \in \mathbb{C}^{N_r \times N_t}$, where the corresponding matrix entries, i.e. $h_{km,ij}^n = [\mathbf{H}_{km}^n]_{ij}$, modeled as independent random variables, account for both large-scale (i.e., path loss and shadowing) and small-scale fading effects. Here, the path loss is modeled as $\mathrm{PL}_{km} = 148.1 + 37.6 \log_{10} d_{km}$(dB) [31], where d_{km} (in km) is the distance between the kth RSU and the mth VUE. Shadowing is modeled using a log-normal distribution, with a standard deviation of 8 dB and zero mean. The log-normal shadowing coefficient is with 8 dB standard derivation and zero mean. The small-scale fading coefficients, denoted by $\xi_{km,ij}^n$, follow the Rayleigh distribution with unit variance and zero mean.

[2]Although we study a multi-antenna scenario in this work, we do not consider multi-antenna issues such as the required number and configuration of the antenna arrays [26] or inter-antenna interference due to mutual coupling [27].

B. Time-Varying Extension

In this work, we aim to investigate the resource allocation problem in a dynamic scenario, where the temporal variations of the channel matrices $\mathbf{H}_{km}^n$ are taken into account. Specifically, it is assumed that the radio channels remain constant within a short time slot of duration Δt, but may change over consecutive time slots, at a rate which depends on the VUEs' mobility and possibly other external factors. To emphasize this time dependence, we specifically denote by $\mathbf{H}_{km}^{n,l}$ the channel matrix between the kth RSU and m VUE on the nth subcarrier at time $t_l = l\Delta t$, where $l \in \{0, 1, 2, \ldots\}$ is the time slot index and Δt is the time interval. In the same way, we use the superscript l to indicate the temporal dependence of other quantities of interest, as in e.g., $\mathbf{X}^l$.

Considering the dynamic nature of the channel state information, we model the time-varying Raleigh coefficients as independent first-order autoregressive processes [32], given by

$$\xi_{km,ij}^{n,l} = \rho_m(\Delta t)\xi_{km,ij}^{n,l-1} + e_{km,ij}^{n,l},$$

where $\rho_m(\Delta t)$ is the channel autocorrelation function and $e_{km,ij}^{n,l}$ is the process noise sequence which is drawn from a $\mathcal{CN}(0, 1 - \rho_m(\Delta t)^2)$ distribution. According to Jakes model, $\rho_m(\Delta t) = J_0(2\pi v_m \Delta t / f_c)$ where $J_0(\cdot)$ is the zero-order Bessel function of the first kind, f_c is the wavelength at the band mid-frequency and v_m is the velocity of the mth VUE.

C. Achievable Data Rate and Power

At time slot l, the received signal of the mth VUE on the nth subcarrier can be expressed as

$$\mathbf{z}_m^{n,l} = \mathbf{H}_{km}^{n,l}\mathbf{V}_{km}^{n,l}\mathbf{y}_m^l + \mathbf{n}_m^l, \tag{3}$$

where $\mathbf{y}_m^l \in \mathbb{C}^{N_s \times 1}$ is the transmitted data and $\mathbf{n}_m^l$ represents additive noise at VUE m, which follows a $\mathcal{CN}(\mathbf{0}, \sigma_m^2\mathbf{I})$ distribution. Accordingly, the achievable data rate of the RSU-VUE pair (k, m) on the nth subcarrier is given by

$$r_{km}^{n,l} = \frac{W}{N} \log \left| \mathbf{I}_{N_r} + \sigma_m^{-2} \mathbf{H}_{km}^{n,l} \mathbf{V}_{km}^{n,l} (\mathbf{V}_{km}^{n,l})^{\mathrm{H}} (\mathbf{H}_{km}^{n,l})^{\mathrm{H}} \right|, \tag{4}$$

where $\log(\cdot)$ is the base-2 logarithm.

Let $\mathbf{V}^l = \{\mathbf{V}_{km}^{n,l}, \forall m, k, n\}$ denote the collection precoding matrices.[3] Thus, the achievable data rate of the mth VUE at time slot l is given by

$$R_m^l(\mathbf{V}^l, \mathbf{X}^l) = \sum_{k=1}^{K} \sum_{n=1}^{N} \pi_{km}^{n,l} r_{km}^{n,l}. \tag{5}$$

Accordingly, the power consumption at the kth RSU is

$$P_k^l(\mathbf{V}, \mathbf{X}) = \sum_{m=1}^{M} \sum_{n=1}^{N} \pi_{km}^{n,l} \left\| \mathbf{V}_{km}^{n,l} \right\|_{\mathrm{F}}^2, \tag{6}$$

while the total power consumption (TPC) of the network is given by

$$P_{\mathrm{tot}}^l(\mathbf{V}^l, \mathbf{X}^l) = \sum_{k=1}^{K} P_k^l, \tag{7}$$

[3]Note that when $\pi_{km}^n = 0$, the corresponding precoding matrix $\mathbf{V}_{km}^n$ needs not be calculated explicitly.

where $P_k^l = P_k^l(\mathbf{V}^l, \mathbf{X}^l)$, i.e., the dependence on $\mathbf{V}^l$ and $\mathbf{X}^l$ is omitted to simplify notations.

D. Problem Formulation

In this work, we approach the resource allocation problem for LTE-based V2I downlink network from the perspective of TPC minimization, under rate constraints. Mathematically, the problem of interest is formulated as follows:

$$\begin{aligned} \text{P1}: \quad & \min_{\mathbf{X}^l, \mathbf{V}^l} \quad P_{\text{tot}}^l \\ & \text{s.t.} \quad \text{C1}: R_m^l \geq R^{\min}, \ \forall m \\ & \qquad \text{C2}: P_k^l \leq P_k^{\max}, \ \forall k \end{aligned} \tag{8}$$

where $R^{\min}$ is the minimum rate requirement of each VUE and $P_k^{\max}$ represents the power budget of the kth RSU. Clearly, Problem P1 represents a temporal sequence of NP-hard combinatorial optimization problems over time slot index l. Previous works did not take into account the possible relationship between the optimal solutions obtained at consecutive time slots and solved each problem independently. However, in this paper, we seek to obtain the optimal resource allocation and precoding schemes at time slot l, as represented by $\mathbf{X}_{\text{opt}}^l$ and $\mathbf{V}_{\text{opt}}^l$, by considering the optimal solutions obtained at the previous time slot, i.e. $\mathbf{X}_{\text{opt}}^{l-1}$ and $\mathbf{V}_{\text{opt}}^{l-1}$.

To solve the dynamic optimization Problem P1 effectively, we propose a novel two-stage algorithm. In the first stage, we exploit the relationship of the optimal solution between different time slots and develop a dynamic resource allocation algorithm based on MDPSO with fixed precoding matrices. In the second stage, we develop a low-complexity algorithm to obtain precoding matrices based on the Lagrange dual method. By combining these two stages, we arrive at the proposed DRA-Pre algorithm, which allows to solve Problem P1 sequentially, as illustrated in Fig. 2.

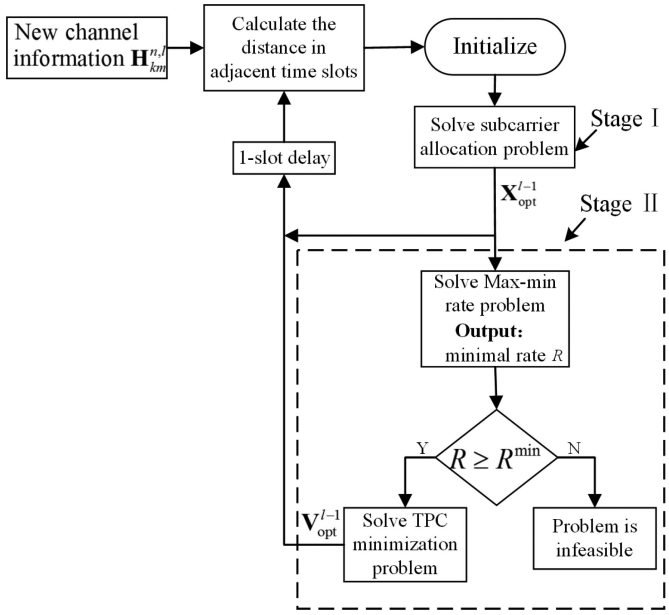

Fig. 2. Overall flowchart of the proposed DRA-Pre algorithm.

III. Stage I: Dynamic Resource Allocation Algorithm

In this section, we investigate the dynamic resource allocation problem with given precoding matrices. Thus, for ease of description, we omit $\mathbf{V}$ from the list of problem variables in the following. To find the optimal resource allocation, an exhaustive search algorithm can be used. However, with K RSUs, M VUEs and N subcarriers, the size of the search space is $\frac{N!}{(N-M)!}K^M M^{N-M}$, which is prohibitive. Hence, for practical applications, we propose a suboptimal resource allocation algorithm with reduced complexity based on MDPSO. In the following, we briefly review the MDPSO method and introduce a distance metric between the optimal resource allocations in adjacent time slots. Then we introduce the proposed MDPSO-based algorithm, along with a discussion of computational complexity.

A. Overview of MDPSO

Particle swarm optimization (PSO) was first developed as a powerful iterative optimization method in [33], inspired by social behavior of bird flocking and fish schooling. MDPSO relies on the use of multiple candidate solutions, called particles and indexed by $i \in \{1, \ldots, I\}$, where I is the swarm size. The state or position of particle i is represented by a multi-value discrete matrix $\boldsymbol{\chi}_i$. The "velocity" of particle i, denoted as $\mathbf{S}_i$, is used to update its position at the next iteration. After each iteration, particle positions are mutated and ultimately, a particle is selected which minimizes the cost or fitness function $f(\boldsymbol{\chi}_i)$.

In particular, for Problem P1, the corresponding fitness function at a given time slot l is represented by

$$f(\boldsymbol{\chi}_i) = P_{\text{tot}}^l(\boldsymbol{\chi}_i), \tag{9}$$

where $\boldsymbol{\chi}_i$ now represents a candidate RSU-VUE pairing and subcarrier allocation, as per the convention in (1). At each time slot, the iterative MDPSO is applied to search an optimal solution minimizing the fitness function (9), where $\tau \in \{0, 1, 2, \cdots\}$ denotes the iteration index. At iteration τ, particles i contains the following information:

- Its velocity $\mathbf{S}_i^\tau$ and position $\boldsymbol{\chi}_i^\tau$.
- The best position $\text{pbest}_i^{\tau'}$, which is the position $\boldsymbol{\chi}_i$ outputting the best fitness value obtained by particle i heretofore, i.e. for $\tau' \in \{1, \ldots, \tau\}$.
- The global best position gbest^τ, which is the particle position yielding the best fitness value among all particles so far.

Note that the iterative procedure stops when a desired level of accuracy or a maximum number of iteration is reached. We point out that as a variant of PSO, the MDPSO algorithm has been shown to outperform the other life emulating algorithms (e.g., genetic algorithms) in terms of efficiency, convergence, complexity [19], [20].

B. Distance Between Optimal Solutions in Adjacent Time Slots

The basic idea advocated here to solve the resource allocation problem in a dynamic environment, is to use information from

previous time slot to facilitate the MDPSO search at the current time slot following a change in channel conditions [18]. This can be achieved in the initialization stage of MDPSO at each time slot by controlling the disperse of the particle on the basis of the expected change in the optimal solution over time. To this end, we need to introduce a measure of the anticipated distance between the optimal resource allocation solutions obtained in adjacent time slots.

In analogy with the Hamming distance, a simple measure of the distance between the optimal solutions at current and previous times l and $l-1$ can be defined as

$$\Delta X^l = \|\mathbf{X}_{\text{opt}}^l - \mathbf{X}_{\text{opt}}^{l-1}\|_d \in [0, N], \tag{10}$$

where the operation $\|\mathbf{A}-\mathbf{B}\|_d$ is interpreted as the number of different rows between matrices $\mathbf{A}$ and $\mathbf{B}$. While such a metric could in theory guide the search of the optimal solution at current time l, in practice $\mathbf{X}_{\text{opt}}^l$ is *a priori unknown* and hence, it is not possible to explicitly calculate ΔX^l in (10).

To bypass this difficulty, we therefore propose to adopt a practical approximation to (10), given by

$$\Delta X^l \approx \left\lfloor \frac{N\sum_{m=1}^{M}\left|R_m^l(\mathbf{X}_{\text{opt}}^{l-1}, \mathbf{H}^l) - R_m^{l-1}(\mathbf{X}_{\text{opt}}^{l-1}, \mathbf{H}^{l-1})\right|}{\sum_{m=1}^{M} R_m^l(\mathbf{X}_{\text{opt}}^{l-1}, \mathbf{H}^{l-1})} \right\rfloor, \tag{11}$$

where $\lfloor\cdot\rfloor$ is the floor operation and $\mathbf{H}^l = \{\mathbf{H}_{km}^{n,l}, \forall k, m, n\}$ is the collection of channel matrices at time slot l. The practical significance of the approximation in (11), which takes into account the previous resource allocation information and the evolution of the channel matrices, can be seen as follows. When the VUEs are moving, their data rates should remain nearly constant; that is, only small changes in the VUEs' data rates are permitted between adjacent time slots. This notion is indeed adequately captured by the right hand side expression in (11).

C. Dynamic Subcarrier Allocation Algorithm

Based on the previous subsections, the details of the dynamic resource allocation algorithm is given in the following.

1) Initialization of the Particles: Note that, at the first time slot (i.e., $l=0$), there is no information from the previous time slot. Thus, all particles are distributed randomly in the solution space. However, for the lth $(l=1,2,\cdots)$ time slot, the algorithm chooses the best position of the previous time slot as the center to disperse and the degree of disperse is restricted by ΔX^l.

The process of disperse at the lth time slot is presented as follows.

1) Generate the matrices $\{\mathbf{Y}_i^l,\ i=1,\ldots,I\}$ by

$$\mathbf{Y}_i^l = \begin{bmatrix} \alpha_{i1} & \beta_{i1} \\ \vdots & \vdots \\ \alpha_{iN} & \beta_{iN} \end{bmatrix} = \text{Mutate}(\mathbf{\Gamma}, \Delta X^l), \tag{12}$$

where $\mathbf{\Gamma} = \mathbf{0}_{N\times 2}$ and the Mutate operation is to randomly select ΔX^l pairs from $\mathbf{\Gamma}$ and reset them to feasible integer values.

2) Obtain particle positions $\{\boldsymbol{\chi}_i^l,\ i=1,\ldots,I\}$ by

$$\boldsymbol{\chi}_i^l = \mathbf{X}_{\text{opt}}^{l-1} + \mathbf{Y}_i^l. \tag{13}$$

The main idea of disperse is to choose ΔX^l pairs from $\mathbf{Y}_i^l$ and change them to random integer values, while the other $(N-\Delta X^l)$ pairs in $\mathbf{Y}_i^l$ remain unchanged. Thus, by dispersing, we can improve the accuracies of the initial solutions and reduce the iteration times remarkably. For notation convenience, we omit the superscript l in the following iteration steps.

2) Update the Particles' Velocities and Positions: In each iteration, particle i updates its velocity $\mathbf{S}_i$ and position $\boldsymbol{\chi}_i$ according to the following expressions [18]:

$$\mathbf{S}_i^{\tau+1} = \varpi_1 \mathbf{S}_i^{\tau} + \varpi_2\ \text{pbest}_i^{\tau} + \varpi_3\ \text{gbest}^{\tau} \tag{14}$$

$$\boldsymbol{\chi}_i^{\tau+1} = \text{Mutate}\ (\mathbf{S}_i^{\tau+1}, \kappa),\ i=1,\ldots,I \tag{15}$$

where the proportional addition operation in (14) is defined in [17]. The basic idea of the operation is to generate new velocities whose elements are selected from the added matrices according to corresponding proportionality coefficients. Typically, ϖ_1 is set to be 1, ϖ_2 and ϖ_3 are distributed uniformly in [0,1]. The Mutation operation is defined in (12) and κ is the mutation coefficient.

3) Obtain the Fitness Value, pbest and gbest: The fitness values can be computed by (9). The calculation of pbest for particle i is given by

$$\text{pbest}_i^{\tau+1} = \begin{cases} \text{pbest}_i^{\tau},\ f(\text{pbest}_i^{\tau}) \le f(\boldsymbol{\chi}_i^{\tau+1}) \\ \boldsymbol{\chi}_i^{\tau+1},\ \text{otherwise} \end{cases} \tag{16}$$

and then the gbest is calculated by

$$\text{gbest}^{\tau+1} = \underset{\{\text{pbest}_i^{\tau+1}\}}{\arg\min}\ f(\text{pbest}_i^{\tau+1}). \tag{17}$$

In conclusion, the MDPSO-based dynamic resource allocation algorithm is given in Algorithm 1.

D. Complexity Analysis

According to the above subsection, the computational complexity of MDPSO-based dynamic resource allocation algorithm mainly lies in three steps: 1) Initialization. 2) Update the positions and velocities. 3) Calculate the fitness value, pbest and gbest. Recall that the swarm size is I and the maximal iteration number is $\tau_{\max}$. In the first step, $2NI$ addition operations are required. In the second step, we need $3I\tau_{\max}$ addition and $2I\tau_{\max}$ multiply operations, respectively. In the third step, $KMNI\tau_{\max}$ addition operations are required. Hence, the total complexity of solving the dynamic resource allocation problem is at most $2I\tau_{\max}$ multiply and $I(2N+3\tau_{\max}+KMN\tau_{\max})$ addition operations.

IV. Stage II: Low-Complexity Precoding Design Algorithm

This section presents a low-complexity algorithm to tackle the precoding problem with $\mathbf{X}_{\text{opt}}^l$ obtained in Stage I. For notation convenience, we omit $\mathbf{X}_{\text{opt}}^l$ in the following. It is worth noting that constraints C1 are non-convex. However,

Algorithm 1 MDPSO-Based Dynamic Resource Allocation at Current Time Slot l.

Initialize the positions and disperse the particles based on the optimal solution of previous time slot $l-1$. Generate feasible $\mathbf{V}$ for all particles such that both constraints C1 and C2 are satisfied. Initialize iteration number $\tau = 1$, and the maximal iteration number is $\tau_{\max}$.
while $\tau \leq \tau_{\max}$ **do**
  for each particle i **do**
    Update its velocity $\mathbf{S}_i^{\tau+1}$ according to (14).
    Update its position $\boldsymbol{\chi}_i^{\tau+1}$ according to (15).
    Update $\text{pbest}_i^{\tau+1}$ according to (16).
  end for
  Update $\text{gbest}^{\tau+1}$ according to (17).
  if $|f(\text{gbest}^{\tau+1}) - f(\text{gbest}^{\tau})|/f(\text{gbest}^{\tau}) < \epsilon$ **then**
    Terminate.
  else
    $\tau = \tau + 1$.
  end if
end while
Output $\mathbf{X}_{\text{opt}}^{l} = \text{gbest}^{\tau+1}$.

this seemingly non-convex problem has many features of convex problems [34]. To exploit it, we introduce new matrix variables $\mathbf{Q}_{km}^n = \mathbf{V}_{km}^n(\mathbf{V}_{km}^n)^{\mathrm{H}} \in \mathbb{C}^{N_t \times N_t}$ and let $\mathbf{Q} = \{\mathbf{Q}_{km}^n, \forall m,k,n\}$. Obviously, $\mathbf{Q}_{km}^n$ is a positive semidefinite matrix and let $\text{rank}(\mathbf{Q}_{km}^n) = \eta_{km}^n$, $\forall k,m,n$. Then, via relaxing rank constraints, the original Problem P1 can be transformed into P2, given by

$$\begin{aligned} \text{P2}: \quad & \min_{\mathbf{Q}} \quad \sum_{k=1}^{K}\sum_{m=1}^{M}\sum_{n=1}^{N} \pi_{km}^n \text{tr}(\mathbf{Q}_{km}^n) \qquad (18) \\ & \text{s.t.} \quad \text{C1}: \sum_{k=1}^{K}\sum_{n=1}^{N} \pi_{km}^n R_{km}^n \geq R^{\min}, \ \forall m \\ & \qquad \text{C2}: \sum_{m=1}^{M}\sum_{n=1}^{N} \pi_{km}^n \text{tr}(\mathbf{Q}_{km}^n) \leq P_k^{\max}, \ \forall k \end{aligned}$$

where $R_{km}^n = \frac{W}{N}\log\left|\mathbf{I}_{N_r} + \sigma_m^{-2}\mathbf{H}_{km}^n\mathbf{Q}_{km}^n(\mathbf{H}_{km}^n)^{\mathrm{H}}\right|$. Denote the optimal solution of P2 by $\mathbf{Q}_{\text{opt}}^{\text{P2}}$. We now conclude Problem P2 is convex. However, P2 may be infeasible because of the conflict between the rate requirements and power constraints. Hence, it is necessary to verify its feasibility, which can be solved by determining whether the minimum rate can satisfy the rate requirement or not.

The problem of checking feasibility is developed into a max-min rate problem, as shown in P3,

$$\begin{aligned} \text{P3}: \quad & \max_{\mathbf{Q}} \quad \min_{m} \quad \sum_{k=1}^{K}\sum_{n=1}^{N} \pi_{km}^n R_{km}^n \qquad (19) \\ & \text{s.t.} \quad \sum_{m=1}^{M}\sum_{n=1}^{N} \pi_{km}^n \text{tr}(\mathbf{Q}_{km}^n) \leq P_k^{\max}, \ \forall k. \end{aligned}$$

The optimal solution and objective value of Problem P3 are denoted by $\mathbf{Q}_{\text{opt}}^{\text{P3}}$ and $R_{\text{opt}}^{\text{P3}}$, respectively. Clearly, if $R_{\text{opt}}^{\text{P3}}$ satisfies the rate requirement, Problem P2 is feasible. Otherwise, it is infeasible. Note that when the solution is infeasible, we will choose $\mathbf{Q}_{\text{opt}}^{\text{P3}}$ as the optimal solution of Problem P2. According to [35], this choice has practical significance. Since when the rate constraints cannot be satisfied, the best choice is trying to achieve the maximum-minimum user rate.

If Problem P2 is feasible, we proceed to solve it by using the Lagrangian dual method. Due to the rank relaxation, the solution of P2 may not be equal to η_{km}^n. This is because the convex feasible set of Problem P2 is a superset of the non-convex feasible set of the rank kept problem. Thus, we devise a new method to solve the rank issue in subsection C. In summary, the algorithm to obtain precoding matrices $\mathbf{V}$ is shown in Stage II of Fig. 2. The remaining tasks are to tackle Problems P2, P3 and the rank issue, respectively.

A. Algorithm to Solve Problem P2

Clearly, Problem P2 can be resolved via typical convex optimization methods (e.g. interior-point method) due to its convexity. However, such a technique undergoes huge complexity and a detailed analysis is given in [36]. Instead, this subsection intends to provide a low-complexity algorithm to tackling P2 through the Lagrangian dual approach.

We first derive the Lagrangian function of P2 with respect to (w.r.t.) the power constraints and rate requirements, written as

$$\begin{aligned} & L_{P2}(\mathbf{Q}, \boldsymbol{\lambda}, \boldsymbol{\mu}) \\ & = \sum_{k=1}^{K}\sum_{m=1}^{M}\sum_{n=1}^{N} \pi_{km}^n \text{tr}(\mathbf{Q}_{km}^n) \\ & \quad + \sum_{m=1}^{M} \lambda_m \left(R^{\min} - \sum_{k=1}^{K}\sum_{n=1}^{N} \pi_{km}^n R_{km}^n \right) \\ & \quad + \sum_{k=1}^{K} \mu_k \left(\sum_{m=1}^{M}\sum_{n=1}^{N} \pi_{km}^n \text{tr}(\mathbf{Q}_{km}^n) - P_k^{\max} \right) \\ & = \sum_{k=1}^{K}\sum_{m=1}^{M}\sum_{n=1}^{N} (2(\mu_k+1)\pi_{km}^n \text{tr}(\mathbf{Q}_{km}^n) - \lambda_m \pi_{km}^n R_{km}^n) \\ & \quad + \sum_{m=1}^{M} \lambda_m R^{\min} - \sum_{k=1}^{K} \mu_k P_k^{\max}, \qquad (20) \end{aligned}$$

where $\boldsymbol{\lambda} = \{\lambda_m \geq 0, \forall m\}$ and $\boldsymbol{\mu} = \{\mu_k \geq 0, \forall k\}$ are the corresponding Lagrangian dual vectors. The dual function is

$$g(\boldsymbol{\lambda}, \boldsymbol{\mu}) = \min_{\mathbf{Q}} L_{P2}(\mathbf{Q}, \boldsymbol{\lambda}, \boldsymbol{\mu}). \qquad (21)$$

Then, the dual problem is described as

$$\max_{\boldsymbol{\lambda}, \boldsymbol{\mu}} g(\boldsymbol{\lambda}, \boldsymbol{\mu}). \qquad (22)$$

The main idea for solving P2 is first to tackle the problem in (21) with given $\boldsymbol{\lambda}$, $\boldsymbol{\mu}$ and then obtain the Lagrangian dual vectors $\boldsymbol{\lambda}$, $\boldsymbol{\mu}$ by tackling the problem in (22).

1) Solving Problem (21): With given $\boldsymbol{\lambda}, \boldsymbol{\mu}$ and after simple calculation, problem (21) can be divided into KMN independent maximization problems, shown as follows.

$$\max_{\mathbf{P}} \log|\mathbf{I}_{N_t} + \mathbf{PA}| - a\text{tr}(\mathbf{P}), \tag{23}$$

where $\mathbf{P} = \mathbf{Q}_{km}^n$, $\mathbf{A} = (\sigma_m^2)^{-1}(\mathbf{H}_{km}^n)^{\text{H}}\mathbf{H}_{km}^n$ and $a = 2(\mu_k + 1)N/(\lambda_m W)$. Here, we use the determinant identity $|\mathbf{I} + \mathbf{AB}| = |\mathbf{I} + \mathbf{BA}|$ and omit the superscripts and subscripts. Firstly, the eigenvalue decomposition (EVD) of $\mathbf{A}$ can be written as

$$\mathbf{A} = \mathbf{UDU}^{\text{H}}, \tag{24}$$

where $\mathbf{U}$ is a unitary matrix of the eigenvectors, $\mathbf{D}$ is a diagonal matrix with $d_1, \ldots, d_r$ being the eigenvalues and $r = \text{rank}(\mathbf{A})$.

Then, by employing the Hadamard inequality [37], the solution of problem (23) is $\mathbf{P} = \mathbf{U}\boldsymbol{\Lambda}\mathbf{U}^{\text{H}}$, where $\boldsymbol{\Lambda} = \text{diag}\{p_1, \ldots, p_i, \ldots, p_r\}$. Taking the derivation of the objective function in (23) w.r.t. p_i, we have

$$p_i = \left[\frac{1}{a} - \frac{1}{d_i}\right]^+, i = 1, \ldots, r,$$

where we define $[x]^+ = \max\{0, x\}$.

Thus, the optimal $\mathbf{Q}_{\text{opt}}^{\text{P2}}$ is written as

$$\mathbf{Q}_{\text{opt}}^{\text{P2}} = \mathbf{U}\boldsymbol{\Lambda}\mathbf{U}^{\text{H}}. \tag{25}$$

2) Solving Problem (22): To tackle problem (22), we adopt the subgradient approach. Note that it is convenient and efficient to deal with the non-differentiable objective function [38]. Then, in the τth iteration, the subgradient can be written as

$$\nabla\lambda_m^\tau = R^{\min} - \sum_{k=1}^{K}\sum_{n=1}^{N}\pi_{km}^n R_{km}^n,\ m = 1, \ldots, M$$

$$\nabla\mu_k^\tau = \sum_{m=1}^{M}\sum_{n=1}^{N}\pi_{km}^n \text{tr}(\mathbf{Q}_{km}^n) - P_k^{\max},\ k = 1, \ldots, K.$$

The update equations for the Lagrangian dual variables are given by

$$\lambda_m^{\tau+1} = \left[\lambda_m^\tau - s_\lambda^\tau \nabla\lambda_m^\tau\right]^+, \forall m, \tag{26}$$

$$\mu_k^{\tau+1} = \left[\mu_k^\tau - s_\mu^\tau \nabla\mu_k^\tau\right]^+, \forall k, \tag{27}$$

where s_λ^τ and s_μ^τ are positive step sizes in the τth iteration. The subgradient approach is proved to converge if s_λ^τ and s_μ^τ satisfy $\lim_{\tau\to\infty} s_\lambda^\tau = 0$ and $\lim_{\tau\to\infty} s_\mu^\tau = 0$, respectively [38]. The algorithm to address Problem P2 is summarized in Algorithm 2.

Algorithm 2: Solving Problem P2.

1: Initialize iteration number $\tau = 1$ and $\boldsymbol{\lambda}^\tau = \mathbf{1}, \boldsymbol{\mu}^\tau = \mathbf{1}$. The maximum iteration number is $\tau_{\max}$. Calculate the objective and denoted by $\text{Obj}_{\text{P2}}^\tau$.
2: **for** Each $\mathbf{Q}_{km}^n, \forall k, m, n$ **do**
3: Compute $\mathbf{Q}_{km}^n = \mathbf{U}\boldsymbol{\Lambda}\mathbf{U}^{\text{H}}$ with fixed $\boldsymbol{\lambda}^\tau, \boldsymbol{\mu}^\tau$ via (25).
4: Update Lagrangian dual vectors $\boldsymbol{\lambda}^\tau, \boldsymbol{\mu}^\tau$ via (26) and (27), respectively.
5: Compute $\text{Obj}_{\text{P2}}^{\tau+1}$.
6: **end for**
7: **if** $|\text{Obj}_{\text{P2}}^{\tau+1} - \text{Obj}_{\text{P2}}^\tau|/\text{Obj}_{\text{P2}}^\tau < \epsilon$ or $\tau > \tau_{\max}$ **then**
8: terminate.
9: **else**
10: set $\tau = \tau + 1$ and go to step 2.
11: **end if**

B. Algorithm to Solve Problem P3

As a well-known max-min rate optimization problem [39], P3 can be solved by introducing an auxiliary variable w and reformulated as follows.

$$\mathbf{P3}: \max_{\mathbf{Q},\omega}\ \omega \tag{28}$$
$$\text{s.t.}\quad \sum_{k=1}^{K}\sum_{n=1}^{N}\pi_{km}^n R_{km}^n \geq \omega,\ \forall m$$
$$\sum_{m=1}^{M}\sum_{n=1}^{N}\pi_{km}^n \text{tr}(\mathbf{Q}_{km}^n) \leq P_k^{\max},\ \forall k.$$

Then, we can also utilize the Lagrangian dual method to tackle Problem P3. The Lagrangian function of P3 is given by

$$\begin{aligned} &L_{P3}(\mathbf{Q}, \omega, \boldsymbol{\phi}, \boldsymbol{\varphi}) \\ &= \omega + \sum_{k=1}^{K}\varphi_k\left(P_k^{\max} - \sum_{m=1}^{M}\sum_{n=1}^{N}\pi_{km}^n \text{tr}(\mathbf{Q}_{km}^n)\right) \\ &\quad + \sum_{m=1}^{M}\phi_m\left(\sum_{k=1}^{K}\sum_{n=1}^{N}\pi_{km}^n R_{km}^n - \omega\right) \\ &= \left(1 - \sum_{m=1}^{M}\phi_m\right)\omega + \sum_{k=1}^{K}\varphi_k P_k^{\max} \\ &\quad + \sum_{k=1}^{K}\sum_{m=1}^{M}\sum_{n=1}^{N}\left(\phi_m\pi_{km}^n R_{km}^n - \varphi_k\pi_{km}^n \text{tr}(\mathbf{Q}_{km}^n)\right), \end{aligned} \tag{29}$$

where $\boldsymbol{\phi} = \{\phi_m \geq 0, \forall m\}$ and $\boldsymbol{\varphi} = \{\varphi_k \geq 0, \forall k\}$ are the corresponding Lagrangian dual vectors. We omit the detailed steps because of the similar procedure with that in solving Problem P2 and only present the final results as follows.

Firstly, the optimal $\mathbf{Q}_{\text{opt}}^{\text{P3}}$ of Problem P3 is given by

$$\mathbf{Q}_{\text{opt}}^{\text{P3}} = \mathbf{U}\boldsymbol{\Lambda}\mathbf{U}^{\text{H}}, \tag{30}$$

where $\boldsymbol{\Lambda} = \text{diag}\{p_1, \ldots, p_i, \ldots, p_r\}$ with

$$p_i = \left[\frac{1}{b} - \frac{1}{d_i}\right]^+, i = 1, \ldots, r,$$

and $b = \varphi_k N/(\phi_m W)$. The definitions of $\mathbf{U}$ and d_i are given in (24).

Algorithm 3: Solving Problem P3.

1: Initialize iteration number $\tau = 1$ and $\omega^\tau = 0, \boldsymbol{\phi}^\tau = \mathbf{1}, \boldsymbol{\varphi}^\tau = \mathbf{1}$. The maximum iteration number is $\tau_{\max}$. Calculate the objective and denoted by $\text{Obj}_{\text{P3}}^\tau$.
2: **for** Each $\mathbf{Q}_{km}^n, \forall k, m, n$ **do**
3: Compute $\mathbf{Q}_{km}^n = \mathbf{U}\boldsymbol{\Lambda}\mathbf{U}^{\text{H}}$ with fixed $\boldsymbol{\phi}^\tau, \boldsymbol{\varphi}^\tau$ via (30).
4: Update $\omega^{\tau+1}$ via (33) and Lagrangian dual vectors $\boldsymbol{\phi}^\tau, \boldsymbol{\varphi}^\tau$ via (31) and (32).
5: Compute $\text{Obj}_{\text{P3}}^{\tau+1}$.
6: **end for**
7: **if** $|\text{Obj}_{\text{P3}}^{\tau+1} - \text{Obj}_{\text{P3}}^\tau|/\text{Obj}_{\text{P3}}^\tau < \epsilon$ or $\tau > \tau_{\max}$ **then**
8: terminate.
9: **else**
10: set $\tau = \tau + 1$ and go to step 2.
11: **end if**

Then, the update equations for the Lagrangian dual variables are given by

$$\phi_m^{\tau+1} = \left[\phi_m^\tau - s_\phi^\tau \left(\sum_{k=1}^{K}\sum_{n=1}^{N} \pi_{km}^n R_{km}^n - \omega^\tau\right)\right]^+, \forall m, \quad (31)$$

$$\varphi_k^{\tau+1} = \left[\varphi_k^\tau - s_\varphi^\tau \left(P_k^{\max} - \sum_{m=1}^{M}\sum_{n=1}^{N} \pi_{km}^n \text{tr}(\mathbf{Q}_{km}^n)\right)\right]^+, \forall k, \quad (32)$$

where s_ϕ^τ and s_φ^τ are positive step sizes in the τth iteration.

It is worthwhile to note that the closed expression optimal ω_{opt} can not be achieved since the Lagrangian function in (29) is linear with ω. Hence, to obtain the optimal ω_{opt}, we propose an iterative equation, given by

$$\omega^{\tau+1} = \omega^\tau - s_\omega^\tau \left(1 - \sum_{m=1}^{M} \phi_m^\tau\right), \quad (33)$$

where s_ω^τ is positive step size in the τth iteration. The algorithm to address Problem P3 is summarized in Algorithm 3.

C. Rank Issue

As mentioned before, Problem P2 may not acquire the optimal solution because of the rank relaxation. In our simulations, we find that Problem P2 always gives higher-rank solutions (i.e., the rank value of $\mathbf{Q}_{km}^n$ is greater than η_{km}^n), which is yet to be proved. Different randomization techniques have been developed to find an approximate from the solution to its relaxed version [40]–[42]. However, the referred papers only consider case $N_s = 1$. Thus, in case of $N_s > 1$, a new technique needs to be devised. Note that, when $N_s = 1$, we can conclude that Problem P2 always produces rank-1 solutions based on Theorem 1.

Theorem 1: Problem P2 always gives rank-1 solutions when $N_s = 1$.

Proof: Obviously, $\text{rank}(\mathbf{Q}_{\text{opt}}^{\text{P2}}) \neq 0$ because of the rate requirements. Thus, to proof Theorem 1, we only need to verify that the rank of $\mathbf{Q}_{\text{opt}}^{\text{P2}}$ is equal to 1. Recall that $\mathbf{H}_{km}^n \in \mathbb{C}^{N_r \times N_t}$ and $N_s = \min\{N_t, N_r\}$. Then, based on (25),

$$\begin{aligned}\text{rank}(\mathbf{Q}_{\text{opt}}^{\text{P2}}) &= \text{rank}(\boldsymbol{\Lambda}) = \text{rank}(\mathbf{A}) \\ &= \text{rank}((\mathbf{H}_{km}^n)^{\text{H}}\mathbf{H}_{km}^n) \\ &\leqslant \min\{N_t, N_r\} = N_s = 1.\end{aligned}$$

Since $\text{rank}(\mathbf{Q}_{\text{opt}}^{\text{P2}}) \neq 0$, we can conclude that $\text{rank}(\mathbf{Q}_{\text{opt}}^{\text{P2}}) = 1$. This completes the proof. ■

Algorithm 4: Solving the Rank Issue.

1: For each solution $\mathbf{Q}_{km}^n$,
2: **if** $\text{rank}(\mathbf{Q}_{km}^n) = \eta_{km}^n$ **then**
3: $\mathbf{V}_{km}^n = \mathbf{L}\boldsymbol{\Sigma}^{1/2}$.
4: **else**
5: $\mathbf{V}_{km}^n = \mathbf{L}_d\boldsymbol{\Sigma}_d^{1/2}$.
6: **end if**

In the following, we propose a modified and simple algorithm to obtain a good solution when the higher-rank solution is produced.

The eigenvalue decomposition of $\mathbf{Q}_{km}^n$ is given by

$$\mathbf{Q}_{km}^n = \mathbf{L}\boldsymbol{\Sigma}\mathbf{L}^{\text{H}}, \quad (34)$$

where $\mathbf{L}$ is a unitary matrix of eigenvectors, $\boldsymbol{\Sigma}$ is a diagonal matrix of eigenvalues. Denote a diagonal matrix whose elements are the d largest eigenvalues by $\boldsymbol{\Sigma}_d$. $\mathbf{L}_d$ is a unitary matrix whose column vectors are the eigenvectors corresponding to the d largest eigenvalues. Then, the method to retrieve the solution is summarized in Algorithm 4.

D. Complexity Analysis

In this subsection, the complexity of solving Problem P2 is analyzed. Because P2 is split into two subproblems, we should analyze the complexity for each one. It is easy to know the main complexity of two algorithms lies in step 4. For Algorithm 2, the computational complexity is $\mathcal{O}(K + M)$. Thus, the complexity of Algorithm 2 is $\mathcal{O}(\tau_{\max}(K + M))$. Similarly, the complexity of Algorithm 3 is $\mathcal{O}(\tau_{\max}(K + M + 1))$. Hence, the total complexity for tackling Problem P2 is at most $\mathcal{O}(\tau_{\max}(K + M + 1))$.

V. Simulation Results

In this section, we evaluate the performance of the proposed DRA-Pre algorithm. In order to make the simulation setup as realistic as possible, we consider a linear highway road in Nanjing with a width of 15 m and length of 2 km.[4] All the RSUs are deployed uniformly on the side of the road, while the VUEs are randomly distributed on the road, each moving at its own constant speed in the range between 40 and 120km/h. The simulation parameters, which are mainly set based on 3GPP TR.36.885 [43], are listed for easy reference in Table II. We denote by $T = L\Delta t$ the whole time interval covered by the simulation experiment,

[4]Here, a four-lane one-way road is considered, where the width of each lane is set to be 3.75 m.

TABLE II
SIMULATION PARAMETERS

Simulation parameters	Value
Total bandwidth W	10 MHz
Number of subcarriers N	32
Band mid-frequency f_c	2 GHz
Time interval Δt	20 ms
Power budget $P_k^{\max}, \forall k$	23 dBm
Rate requirement $R^{\min}$	0.1 Mbps
Number of RSUs K	20
Number of VUEs M	20
Number of transmitting antennas N_t	4
Number of receiving antennas N_r	2
Number of data streams N_s	2
Thermal noise power $\sigma_m^2, \forall m$	-174 dBm/Hz
Swarm size I	50
Maximal iteration number $\tau_{\max}$	200
Mutation factor κ	2

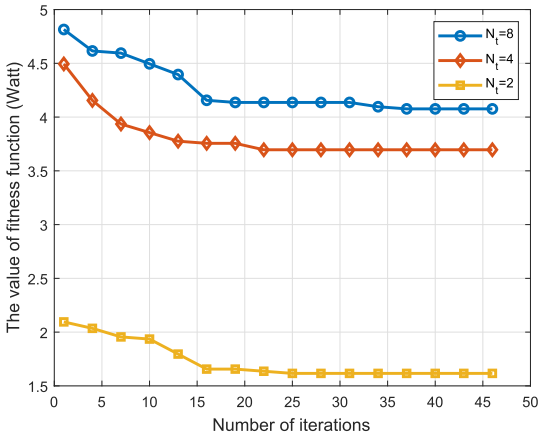

Fig. 3. Convergence behavior of Algorithm 1 when solving resource allocation problem under different numbers of transmitting antennas.

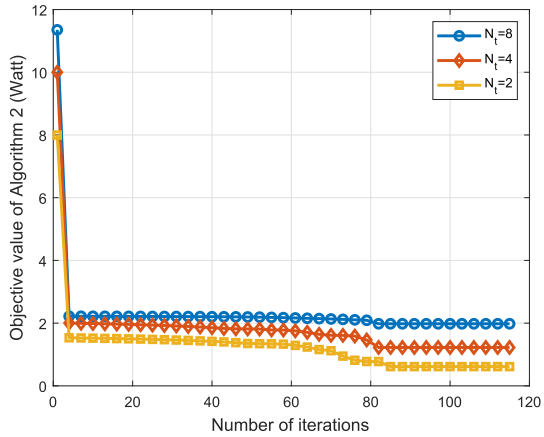

Fig. 4. Convergence behavior of Algorithm 2 when solving Problem P2 under different numbers of transmitting antennas.

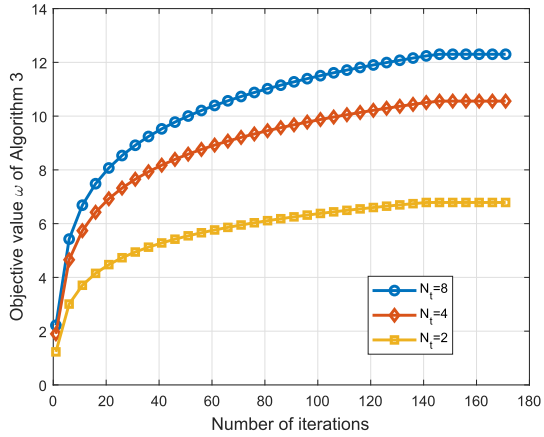

Fig. 5. Convergence behavior of Algorithm 3 when solving Problem P3 under different numbers of transmitting antennas.

where Δt is the time slot duration and L is the total number of slots.

A. Properties of the Proposed Algorithms

1) Convergence Behaviors of the Proposed Algorithms: In this subsection, we present the simulation results to study the convergence behaviors of Algorithms 1, 2 and 3. The results are obtained under three different configurations: the RSUs with $N_t = 2$, $N_t = 4$ and $N_t = 8$.

Fig. 3 shows the convergence behavior of Algorithm 1 under diverse N_t. It can be seen from Fig. 3 that the fitness value in (9) decreases with the iteration number and converges fast. As expected, the converged fitness value increases with N_t.

Figs. 4 and 5 illustrate the convergence behaviors of Algorithm 2 and 3, respectively. According to the simulation experiments, the step sizes in Algorithm 2 are set as $s_\lambda^\tau = (3e^5\tau)^{-1}$ and $s_\nu^\tau = (3e^2\tau)^{-1}$, where τ is the iteration index. For Algorithm 3, the step sizes are respectively set as $s_\omega^\tau = (30\tau)^{-1}$, $s_\phi^\tau = (3e^5\tau)^{-1}$ and $s_\varphi^\tau = (3e^4\tau)^{-1}$. It can be seen from two figures that the power consumption decreases with the iteration number, while the objective ω in Problem P3 increases. Additionally, the converged values in both Algorithm 2 and 3 are marginally affected by the number of the transmitting antennas.

2) Impacts of the Numbers of RSUs and VUEs: In Figs. 6 and 7, the impacts of the numbers of RSUs and VUEs on the TPC are studied when $T = 20$ ms. On the one hand, the TPC increases with the rate requirements under two scenarios as expected. On the other hand, we find that the TPC decreases with the number of RSUs in Fig. 6. The reasons can be explained as follows. Firstly, when the network consists of plenty of RSUs, the average distance between the RSU and VUE is reduced. As a consequence, each RSU only needs to consume a small amount of power to meet the rate requirements. Secondly, the active number of RSU may decrease with the number of RSUs.

Fig. 7 indicates that the TPC increases with the rate requirement, only slightly when $M = 20$ and $M = 25$, but more significantly when $M = 30$. The reason is that with the increase of rate requirement, more RSUs will be active to serve the large number of VUEs, which requires a large quantity of power consumption. In other words, when the number of VUE is moderate, a small number of RSUs can satisfy the rate requirement.

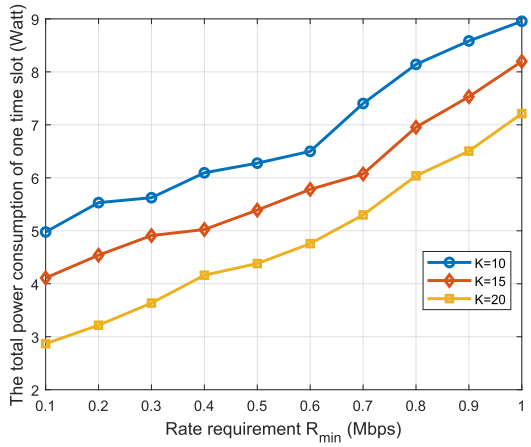

Fig. 6. TPC versus the rate requirements under the different numbers of RSUs with $M = 20$.

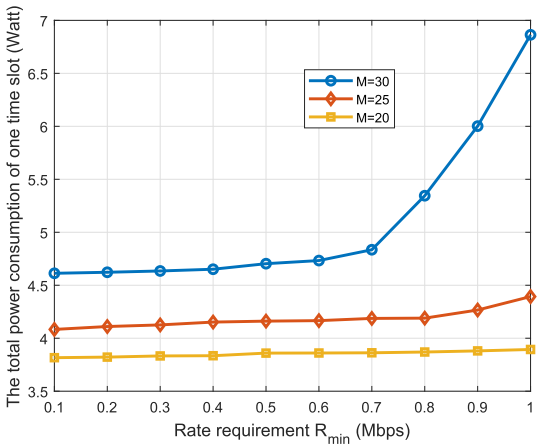

Fig. 7. TPC versus the rate requirements under the different numbers of VUEs with $K = 20$.

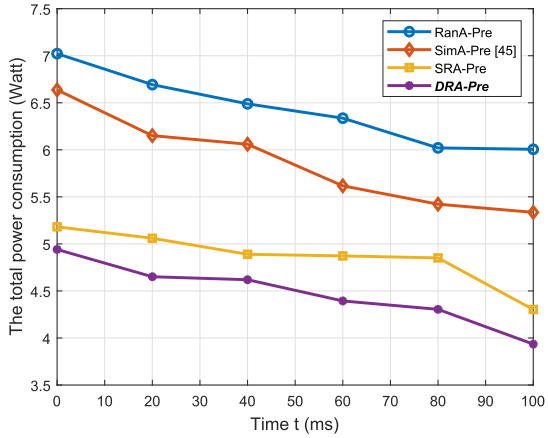

Fig. 8. TPC versus the time period T, where $M = K = 20$ and $R_{\min} = 0.1$ Mbps.

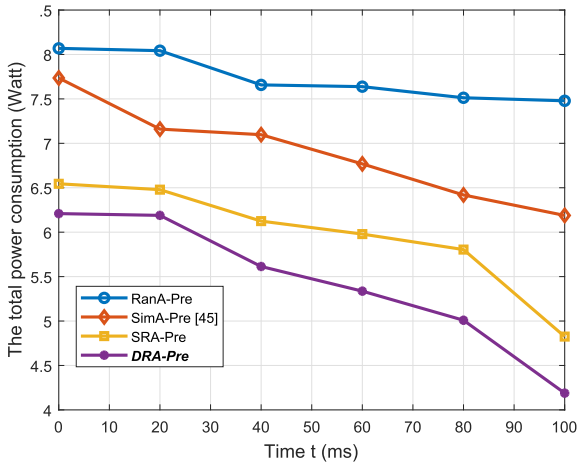

Fig. 9. TPC versus the time period T, where $M = K = 20$ and $R_{\min} = 0.5$ Mbps.

B. Performance Comparison and Analysis

In this subsection, we study the performance comparison among the following four schemes:

1) The proposed DRA-Pre, shown in Fig. 2.
2) The static resource allocation and precoding algorithm, named SRA-Pre, which does not use the information of each time slot. In other words, at each time slot, we do not need to compute ΔX and solve each problem independently.
3) Random resource allocation in Stage I, named RanA-Pre. For each subcarrier, we allocate RSU-VUE pair randomly during each time slot.
4) Simulated annealing[5] based resource allocation and precoding algorithm [45], named SimA-Pre. This method includes two major steps: the generation of a neighbor $\mathbf{X}$ and determination of TPC.

[5]In general, the PSO method is faster than the simulated annealing one since the PSO contains parallel search techniques [44].

In Figs. 8 and 9, the TPC performance of four schemes at different rate requirement are illustrated. Obviously, the proposed DRA-Pre outperforms the other algorithms, regardless of the rate requirement. The reason is that DRA-Pre exploits the information of each time slot. In other words, to achieve better TPC performance, the information of the previous time slot should be utilized to obtain a new resource allocation strategy. Additionally, form Figs. 8 and 9, we can see that the TPC at $R_{\min} = 10$ kbps is higher than that at $R_{\min} = 3$ kbps, which is keeping with the phenomenon of Fig. 6. The reason can be explained as follows. To satisfy a higher rate requirement, each RSU needs to transmit with more power, which is consistent with the reality.

In Figs. 8 and 10, the TPC of four schemes at different number of VUEs are presented. Clearly, our proposed DRA-Pre algorithm achieves the best TPC performance among all the algorithms. In addition, the TPC in the case of $M = 20$ is lower than that of $M = 25$, which is consistent with the phenomenon in Fig. 7.

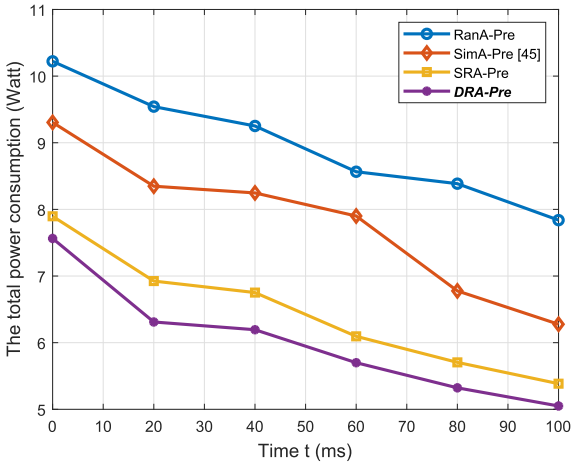

Fig. 10. TPC versus the time period T, where $K = 20$, $M = 25$, and $R_{\min} = 0.1$ Mbps.

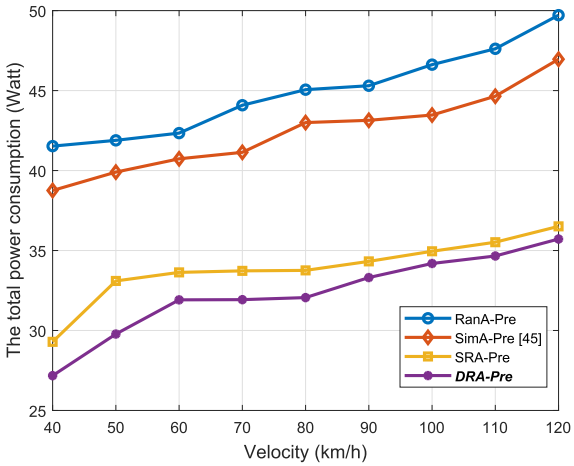

Fig. 11. TPC under the different velocities of VUEs, where $T = 100$ ms.

Fig. 11 shows that the TPC of four algorithms under the different velocities of VUEs. For the sake of simulation, we assume that all the VUEs are at the same speed. It can be seen that the proposed algorithm is superior to the other three algorithms, regardless of the velocity and the TPC increases slightly with the velocity. In addition, when the velocity is greater than 90 km/h, the proposed DRA-Pre provides marginal TPC performance than the SRA-Pre. The reasons can be explained as follows. Firstly, many VUEs will leave the road segment quickly when they are at high speed. In other words, as the distances between VUEs and RSUs increase, the RSUs should transmit with more power to satisfy the rate requirements. Secondly, the relationship between adjacent time slots is diminished with the increasing velocity, which is consistent with the analysis in [18]. To further study the impacts of time interval Δt on performance variation between the proposed DRA-Pre and static SRA-Pre, we simulate the TPC under different Δt, as shown in Fig. 12. As expected, the smaller Δt, the higher performance gain DRA-Pre provides. The reason can be explained as follows. The communication environment changes rapidly with the moving speed.

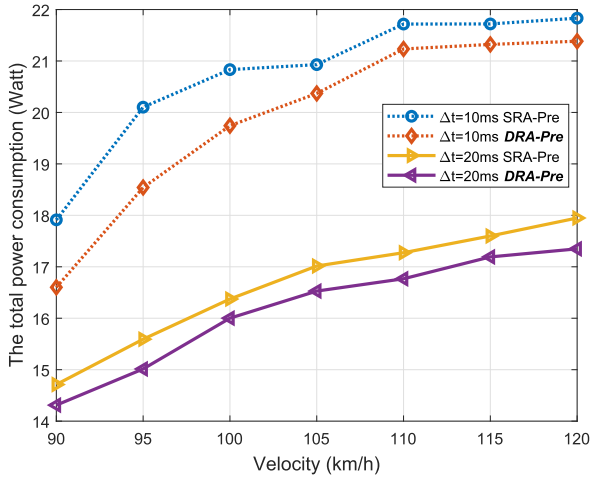

Fig. 12. TPC under the different velocities of VUEs and time interval, where $T = 60$ ms.

Thus, the proposed DRA-Pre can capture the dynamic characteristic with a smaller Δt.

VI. Conclusion

In this paper, we investigated the dynamic resource allocation (i.e., RUS-VUE pairing and subcarrier allocation) and precoding joint design problem for LTE-based V2I networks, where the objective is to minimize the TPC. Under time-varying channel conditions, the TPC minimization problem takes the form of discrete-time sequence of NP-hard combinational optimization problems. To improve the tractability, we split the original problem into resource allocation problem (Stage I) and precoding design problem (Stage II). In the first stage, we proposed a dynamic resource allocation algorithm based on MPDSO, where we exploited the relationship between resource allocation solutions in adjacent time slots to improve the TPC performance. Considering the conflicting requirements between the rate and power constraints, we first checked the feasibility by solving a max-min rate problem in the second stage. Then, we proposed a low-complexity algorithm to tackle the precoding problem through splitting it into two subproblems and the Lagrangian dual method. By combining these two stages, we propose a dynamic resource allocation and precoding algorithm (DRA-Pre). Simulation results illustrated that our proposed DRA-Pre algorithm can achieve better TPC performance compared with the existing methods.

References

[1] S. Chen, J. Hu, Y. Shi, and L. Zhao, "LTE-V: A TD-LTE-based V2X solution for future vehicular network," *IEEE Int. Things J.*, vol. 3, no. 6, pp. 997–1005, Dec. 2016.

[2] G. Araniti, C. Campolo, M. Condoluci, A. Iera, and A. Molinaro, "LTE for vehicular networking: A survey," *IEEE Commun. Mag.*, vol. 51, no. 5, pp. 148–157, May 2013.

[3] S. H. Sun, J. L. Hu, Y. Peng, X. M. Pan, L. Zhao, and J. Y. Fang, "Support for Vehicle-to-Everything services based on LTE," *IEEE Wireless Commun.*, vol. 23, no. 3, pp. 4–8, Jun. 2016.

[4] H. Seo, K. D. Lee, S. Yasukawa, Y. Peng, and P. Sartori, "LTE evolution for vehicle-to-everything services," *IEEE Commun. Mag.*, vol. 54, no. 6, pp. 22–28, Jun. 2016.
[5] G. Karagiannis *et al.*, "Vehicular networking: A survey and tutorial on requirements, architectures, challenges, standards and solutions," *IEEE Commun. Surv. Tut.*, vol. 13, no. 4, pp. 584–616, Oct.–Dec. 2011.
[6] K. Zheng, Q. Zheng, P. Chatzimisios, W. Xiang, and Y. Zhou, "Heterogeneous vehicular networking: A survey on architecture, challenges, and solutions," *IEEE Commun. Surv. Tut.*, vol. 17, no. 4, pp. 2377–2396, Oct.–Dec. 2015.
[7] S. Chen *et al.*, "Vehicle-to-Everything (v2x) services supported by LTE-based systems and 5G," *IEEE Commun. Standards Mag.*, vol. 1, no. 2, pp. 70–76, Jul. 2017.
[8] "Global mobile data traffic forecast update, 2016–2021," C. V. N. I. Cisco, San Jose, CA, USA, Feb. 2017.
[9] L. Liang, H. Peng, G. Y. Li, and X. Shen, "Vehicular communications: A physical layer perspective," *IEEE Trans. Veh. Technol.*, vol. 66, no. 12, pp. 10647–10659, Dec. 2017.
[10] L. Liang, H. Ye, and G. Y. Li, "Towards intelligent vehicular networks: A machine learning framework," *IEEE Internet Things J.*, vol. 6, no. 1, pp. 124–135, Feb. 2019.
[11] Z. Kuang, Z. Chen, J. Pan, and D. Sajjadi, "Joint optimization of spectrum access and power allocation in uplink OFDMA CR-VANETs," *Wireless Netw.*, vol. 25, pp. 1–11, 2019. [Online]. Available: https://doi.org/10.1007/s11276-017-1537-7
[12] M. Tabassum, M. A. Razzaque, M. M. Hassan, A. Almogren, and A. Alamri, "Interference-aware high-throughput channel allocation mechanism for CR-VANETs," *EURASIP J. Wireless Commun. Netw.*, vol. 2016, no. 1, pp. 1–15, 2016.
[13] S. Y. Pyun, W. Lee, and D. H. Cho, "Resource allocation for vehicle-to-infrastructure communication using directional transmission," *IEEE Trans. Intell. Transp. Syst.*, vol. 17, no. 4, pp. 1183–1188, Apr. 2016.
[14] H. Peng *et al.*, "Resource allocation for cellular-based inter-vehicle communications in autonomous multiplatoons," *IEEE Trans. Veh. Technol.*, vol. 66, no. 12, pp. 11249–11263, Dec. 2017.
[15] L. Liang, J. Kim, S. C. Jha, K. Sivanesan, and G. Y. Li, "Spectrum and power allocation for vehicular communications with delayed CSI feedback," *IEEE Wireless Commun. Lett.*, vol. 6, no. 4, pp. 458–461, Aug. 2017.
[16] L. Liang, G. Y. Li, and W. Xu, "Resource allocation for D2D-enabled vehicular communications," *IEEE Trans. Commun.*, vol. 65, no. 7, pp. 3186–3197, Jul. 2017.
[17] W. Li, S. Zeng, Z. Jin, Q. Xin, and J. Lei, "Particle swarm optimization based resource allocation and adaptive modulation in cooperative OFDMA systems," in *Proc. IEEE Int. Conf. Comput. Commun.*, 2013, pp. 1–6.
[18] W. Li, J. Lei, T. Wang, C. Xiong, and J. Wei, "Dynamic optimization for resource allocation in relay-aided OFDMA systems under multiservice," *IEEE Trans. Veh. Technol.*, vol. 65, no. 3, pp. 1303–1313, Mar. 2016.
[19] M. Khan, R. S. Alhumaima, and H. S. Al-Raweshidy, "QoS-aware dynamic RRH allocation in a self-optimized cloud radio access network with RRH proximity constraint," *IEEE Trans. Netw. Serv. Manage.*, vol. 14, no. 3, pp. 730–744, Sep. 2017.
[20] M. Khan, Z. H. Fakhri, and H. S. Al-Raweshidy, "Semistatic cell differentiation and integration with dynamic BBU-RRH mapping in cloud radio access network," *IEEE Trans. Netw. Serv. Manage.*, vol. 15, no. 1, pp. 289–303, Mar. 2018.
[21] S. Pyun, D. Cho, and J. Son, "Downlink resource allocation scheme for smart antenna based V2V2I communication system," in *Proc. IEEE Veh. Technol. Conf.*, Sep. 2011, pp. 1–6.
[22] T. Nguyen, O. Berder, and O. Sentieys, "Energy-efficient cooperative techniques for infrastructure-to-vehicle communications," *IEEE Trans. Intell. Transp. Syst.*, vol. 12, no. 3, pp. 659–668, Sep. 2011.
[23] M. M. Mowla, I. Ahmad, D. Habibi, and Q. V. Phung, "A green communication model for 5G systems," *IEEE Trans. Green Commun. Netw.*, vol. 1, no. 3, pp. 264–280, Sep. 2017.
[24] T. Villa, R. Merz, and R. Knopp, "Dynamic resource allocation in heterogeneous networks," in *Proc. IEEE Global Commun. Conf.*, Dec. 2013, pp. 1915–1920.
[25] M. Y. Lyazidi, N. Aitsaadi, and R. Langar, "Dynamic resource allocation for cloud-RAN in LTE with real-time BBU/RRH assignment," in *Proc. IEEE Int. Conf. Commun.*, May 2016, pp. 1–6.
[26] D. Phan-Huy *et al.*, "5G on board: How many antennas do we need on connected cars?" in *Proc. IEEE Globecom Workshops*, Dec. 2016, pp. 1–7.
[27] M. Melvasalo, P. Janis, and V. Koivunen, "MMSE equalizer and chip level inter-antenna interference canceler for HSDPA MIMO systems," in *Proc. IEEE Veh. Technol. Conf.*, May 2006, vol. 4, pp. 2008–2012.
[28] P. Ferrand, A. Decurninge, M. Guillaud, and L. Ordonez, "Efficient channel state information acquisition in massive MIMO systems using non-orthogonal pilots," in *Proc. Int. ITG Workshops Smart Antennas*, Mar. 2017, pp. 1–8.
[29] H. Suzuki, R. Kendall, C. K. Sung, and D. Humphrey, "Efficient and accurate channel feedback for multi-user MIMO-OFDMA," in *Proc. Int. Symp. Commun. Inf. Technol.*, Sep. 2017, pp. 1–6.
[30] L. Zheng and D. N. C. Tse, "Diversity and multiplexing: A fundamental tradeoff in multiple-antenna channels," *IEEE Trans. Inf. Theory*, vol. 49, no. 5, pp. 1073–1096, May 2003.
[31] "Evolved universal terrestrial radio access (e-utra); further advancements for e-utra physical layer aspects," 3GPP, Sophia Antipolis Cedex, France, Tech. Rep. 3GPP TR 36.814, 2017. [Online]. Available: http://www.3gpp.org/DynaReport/36814.htm
[32] A. Goldsmith, *Wireless Communications*. Cambridge, U.K.: Cambridge Univ. Press, 2005.
[33] J. Kennedy and R. Eberhart, "Particle swarm optimization," in *Proc. IEEE Int. Conf. Neural Netw.*, Nov. 1995, vol. 4, pp. 1942–1948.
[34] Z.-Q. Luo and W. Yu, "An introduction to convex optimization for communications and signal processing," *IEEE J. Sel. Areas Commun.*, vol. 24, no. 8, pp. 1426–1438, Aug. 2006.
[35] J. Xu and L. Qiu, "Energy efficiency optimization for MIMO broadcast channels," *IEEE Trans. Wireless Commun.*, vol. 12, no. 2, pp. 690–701, Jan. 2013.
[36] H. Ren, N. Liu, C. Pan, and C. He, "Energy efficiency optimization for MIMO distributed antenna systems," *IEEE Trans. Veh. Technol.*, vol. 66, no. 3, pp. 2276–2288, Mar. 2017.
[37] D. Hoang and R. A. Iltis, "Noncooperative eigencoding for MIMO ad hoc networks," *IEEE Trans. Signal Process.*, vol. 56, no. 2, pp. 865–869, Feb. 2008.
[38] D. P. Palomar and M. Chiang, "A tutorial on decomposition methods for network utility maximization," *IEEE J. Sel. Areas Commun.*, vol. 24, no. 8, pp. 1439–1451, Aug. 2006.
[39] X. Wang and X.-D. Zhang, "Linear transmission for rate optimization in MIMO broadcast channels," *IEEE Trans. Wireless Commun.*, vol. 9, no. 10, pp. 3247–3257, Sep. 2010.
[40] K. T. Phan, S. A. Vorobyov, N. D. Sidiropoulos, and C. Tellambura, "Spectrum sharing in wireless networks via QoS-aware secondary multicast beamforming," *IEEE Trans. Signal Process.*, vol. 57, no. 6, pp. 2323–2335, Jun. 2009.
[41] S. Timotheou, I. Krikidis, G. Zheng, and B. Ottersten, "Beamforming for MISO interference channels with QoS and RF energy transfer," *IEEE Trans. Wireless Commun.*, vol. 13, no. 5, pp. 2646–2658, May 2014.
[42] M. M. Zhao, Y. Cai, Q. Shi, B. Champagne, and M. J. Zhao, "Robust transceiver design for MISO interference channel with energy harvesting," *IEEE Trans. Signal Process.*, vol. 64, no. 17, pp. 4618–4633, Sep. 2016.
[43] "Study on LTE-based V2X services, version 1.0.0," 3GPP, Sophia Antipolis Cedex, France, Tech. Rep. 3GPP TR. 36.885, Jul. 2016. [Online]. Available: http://www.3gpp.org/DynaReport/36885.htm
[44] H.-L. Shieh, C.-C. Kuo, and C.-M. Chiang, "Modified particle swarm optimization algorithm with simulated annealing behavior and its numerical verification," *Appl. Math. Comput.*, vol. 218, no. 8, pp. 4365–4383, 2011. [Online]. Available: http://www.sciencedirect.com/science/article/pii/S0096300311012422
[45] S. Dadallage, C. Yi, and J. Cai, "Joint beamforming, power, and channel allocation in multiuser and multichannel underlay MISO cognitive radio networks," *IEEE Trans. Veh. Technol.*, vol. 65, no. 5, pp. 3349–3359, May 2016.

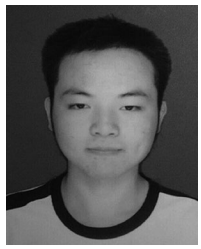

Jianfeng Shi received the B.S. degree in communication engineering from Nanjing Normal University, Nanjing, China, in 2014. He is currently working toward the Ph.D. degree with the National Mobile Communication Research Laboratory, Southeast University, Nanjing, China. From September 2017 to September 2018, he was a Visiting Student with the Department of Electrical Computer Engineering, McGill University, Canada. From 2015 to 2018, he was a TPC member of the IEEE International Conference on Communications (ICC), Wireless Communications and Networking Conference (WCNC), and International Conference on Communications in China (CIC ICCC). His research interest includes D2D communication, user-centric networks, and dynamic optimization.

Zhaohui Yang received the B.S. degree in information science and engineering from Chien-Shiung Wu Honors College, Southeast University, Nanjing, China, in 2014, and the Ph.D. degree in communication and information system from the National Mobile Communications Research Laboratory, Southeast University, Nanjing, China, in 2018. He is currently a Postdoctoral Research Associate with the Center for Telecommunications Research, Department of Informatics, King's College London, London, U.K. His research interests include full-duplex, UAV, URLLC, IoT, edge computing, energy harvesting, and non-orthogonal multiple access. He was a TPC member of the IEEE ICC from 2015 to 2018 and Globecom from 2017 to 2018.

Hao Xu received the B.S. degree in communication engineering from the Nanjing University of Science and Technology, Nanjing, China, in 2013. He is currently working toward the Ph.D. degree with National Mobile Communications Research Laboratory, Southeast University, Nanjing, China. Since September 2016, he has been a Visiting Student with the School of Electrical and Computer Engineering, Georgia Institute of Technology, Atlanta, GA, USA. His research interests mainly include D2D communication, robust transceiver designs, and energy efficiency optimization in wireless networks.

Ming Chen received the B.Sc., M.Sc., and Ph.D. degrees in mathematics from Nanjing University, Nanjing, China, in 1990, 1993, and 1996, respectively. In July 1996, he joined the National Mobile Communications Research Laboratory, Southeast University, Nanjing, China, as a Lecturer. From April 1998 to March 2003, he was an Associate Professor and since April 2003, and he has been a Professor with the Laboratory. His research interests include signal processing and radio resource management of mobile communication systems.

Benoit Champagne received the B.Ing. degree in engineering physics from the Ecole Polytechnique of Montreal, Montreal, Canada, in 1983, the M.Sc. degree in physics from the University of Montreal, Montreal, Canada, in 1985, and the Ph.D. degree in electrical engineering from the University of Toronto, Toronto, ON, Canada, in 1990. From 1990 to 1999, he was an Assistant Professor and then an Associate Professor with National Institute of Scientific Research (INRS)-Telecommunications, Montreal. In 1999, he joined McGill University, Montreal, QC, Canada, where he is currently a Full Professor with the Electronics and Communication Engineering Department. His research interests include statistical signal processing and wireless communications, where he has coauthored more than 250 publications. He has been an Associate Editor for the IEEE SIGNAL PROCESSING LETTERS and the IEEE TRANSACTIONS ON SIGNAL PROCESSING.